# Overcoming Current Quantization Effects for Precise Current Control by Combining Dithering Techniques and Kalman Filter

Hongzhong Zhu and Hiroshi Fujimoto
Department of Electrical Engineering, The University of Tokyo
5-1-5 Kashiwanoha, Kashiwa, Chiba, 277-8561, Japan
Email: zhu@hflab.k.u-tokyo.ac.jp, fujimoto@k.u-tokyo.ac.jp

***Abstract*—Accurate current signals are required for precise current control of AC motor drives. However, current measurement error including the metering error and the quantization error is unavoidable due to the inaccuracy of current sensors and the quantizing feature of analog-to-digital converters. In this paper, the combination of dithering techniques and Kalman filter is presented to suppress the current quantization effects caused by A/D converters. Firstly, the dithering system is designed to whiten the total current measurement error. Then, Kalman filter is exploited to estimate the real current signals from the whitened noise. The effectiveness of the proposed approach is verified via simulations and experiments using a high-precision stage.**

## I. Introduction

Precise current measurement is essential for current control of AC motor drives to produce high static and dynamic performance of ac motor drive systems. As the current measurement error is introduced into the control system by current sensors and A/D converters (ADCs), the real current signals of a motor are not guaranteed to follow the reference values exactly. This would cause torque ripple and deteriorate the control performance especially when motor works at low load [1], [2]. Therefore, to understand and suppress the current measurement error have attracted a great deal of attention.

Fig. 1 shows the typical path of the current measurement for current control. Current signals, which are generated by current sensors, are transformed into digital values via A/D converters after the amplitude amplification and noise filtering. During this procedure, the metering noise and the quantization error are introduced into the control system, as indicated in Fig. 2. The metering noise, denoted by $\eta$, is mainly caused by thermal drift of analog devices of the measurement system. The quantization error, denoted by $q$, arises because the analog current signal may assume any value within the input range of the A/D converters while the output data are finite precision samples. Quantization error behaves as highly colored noise and cannot be ignored in many cases. Some observer-based methods are proposed to suppress the quantization effects [4]. However, the robustness against the input disturbance and the measurement error is usually not taken into account. It is reported that quantization error would affect the accuracy of the rotor position estimation when high frequency signal injection method is used for sensorless control [3].

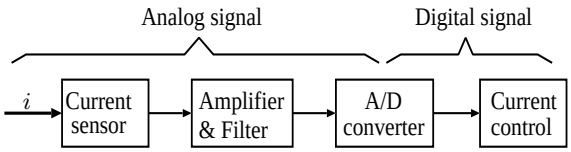


Fig. 1. Path of current measurement.

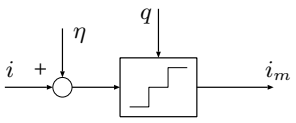


Fig. 2. Model of the current measurement: $\eta$ is the metering noise, and $q$ is the quantization error.

It is well-known that white noise is easier to be reduced than other colored noise because it contains equal power at any center frequency. Many methods, such as Kalman filter and LQG controller design methods, are powerful especially if the noise introduced into the system is white [5]. Motivated by this perspective, in this paper, dither systems are designed to whiten the current quantization noise by taking into account the statistical properties of the metering noise. Furthermore, in order to reduce the whitened measurement noise, Kalman filter is also presented to estimate the real current value to enhance the control performance.

The remainder of this paper is organized as follows. Section II introduces the model of plant and presents some important theorems referring to quantization and dither. The dithering techniques and Kalman filter for suppressing quantization noise are proposed in Section III. Sections IV and V demonstrate the effectiveness of the proposed extended dithering techniques via simulations and experiments. Finally, conclusion is given in Section VI.

For simplicity, the following notations are used in this study:

| | |
|---|---|
| $R$ | Stator resistance per phase, Ω; |
| $L$ | Stator inductance, H; |
| $J$ | Inertia of mass, kg·m$^2$; |
| $B$ | Viscosity, N·m/(rad/s); |
| $K_t$ | Torque coefficient, N·m/A; |
| $K_e$ | Back-EMF constant, V·rad/s; |
| $T$ | Torque, N·m; |

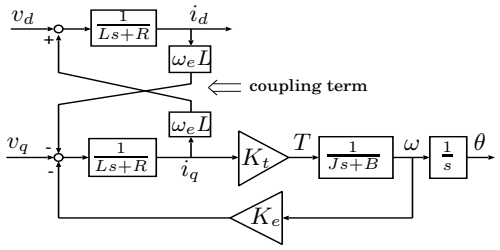


Fig. 3. Model of surface PM synchronous motor.

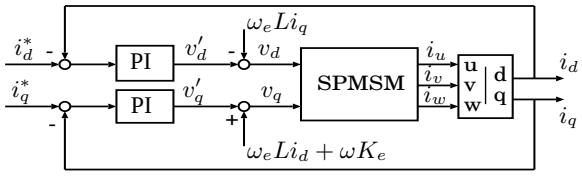


Fig. 4. Current control of SPMSM.

| | |
|---|---|
| $\omega$ | Motor speed, rad/s; |
| $\omega_e$ | field angular speed, rad/s; |
| $\theta$ | Motor angular, rad; |
| $\theta_e$ | field angular, rad; |
| $v_x$ | $x$($u$ or $v$ or $w$)-phase/($d$ or $q$)-axis voltage, V; |
| $i_x$ | $x$($u$ or $v$ or $w$)-phase/($d$ or $q$)-axis current, A; |
| $s$ | Laplace operator; |

## II. Preliminaries

### A. System model

Current control for a surface PM synchronous motor (SPMSM) is considered, and $d, q$-axis voltage equations can be expressed by [2]

$$\begin{bmatrix} v_d \\ v_q \end{bmatrix} = \begin{bmatrix} Ls+R & -\omega_e L \\ \omega_e L & Ls+R \end{bmatrix} \begin{bmatrix} i_d \\ i_q \end{bmatrix} + \omega K_e \begin{bmatrix} 0 \\ 1 \end{bmatrix}. \quad (1)$$

The model is shown in Fig. 3. Generally, PI control approach with decoupling control is exploited for current control. Fig. 4 shows the control block diagram. For the sake of convenience, the fictive indexes $v_d'$ and $v_q'$ are introduced that

$$v_d' \triangleq v_d + \omega_e L i_q, \quad (2)$$

$$v_q' \triangleq v_q - (\omega_e L i_d + \omega K_e). \quad (3)$$

According to the coordinate transformation, the following equation can be obtained:

$$\begin{bmatrix} i_u \\ i_v \\ i_w \end{bmatrix} = \frac{2}{3}\frac{1}{Ls+R} \begin{bmatrix} 1 & -\frac{1}{2} & -\frac{1}{2} \\ -\frac{1}{2} & 1 & -\frac{1}{2} \\ -\frac{1}{2} & -\frac{1}{2} & 1 \end{bmatrix} \begin{bmatrix} v_u' \\ v_v' \\ v_w' \end{bmatrix}, \quad (4)$$

where $[v_u'\ v_v'\ v_w']^T$ is the fictive voltage vector obtained from $[v_d'\ v_q']^T$ by coordinate transformation.

As indicated in the Section 1, current signals are quantized by ADCs before they are used for control. An ideal ADC is a nonlinear device having a staircase-type I/O relation, as shown in Fig. 5. Assuming that the input is always within the measurement range of ADCs, the output $y$ can be expressed in terms of the input $x$ as

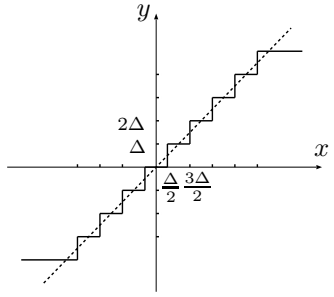


Fig. 5. Quantization characteristic. $\Delta$ is the quantization step.

$$y = Q(x) = \Delta \left\lfloor \frac{x}{\Delta} + \frac{1}{2} \right\rfloor, \quad (5)$$

where $Q(\cdot)$ is the quantizing operation, $\lfloor \cdot \rfloor$ is the floor operator, and $\Delta$ is the quantization step defined by

$$\Delta = \frac{I_0}{2^{N_b - 1}}, \quad (6)$$

where $I_0$ is the one-sided measurement range of current sensor, and $N_b$ is the resolution of an A/D converter. The quantization error is defined by

$$q \triangleq Q(x) - x. \quad (7)$$

$q$ is dependent of $x$ unless $x$ satisfies the so-called band-limited condition, which is also referred to as the "Quantization Theorem" [9]. Although $q$ is usually highly colored, its classical model treats it as a random process with a probability density function (pdf) [7]

$$p_q(\epsilon) = \begin{cases} \frac{1}{\Delta}, & -\frac{\Delta}{2} < \epsilon \leq \frac{\Delta}{2} \\ 0, & \text{otherwise.} \end{cases} \quad (8)$$

Based on this treatment, the mean and the variance of the quantization error are

$$E[q] = 0, \quad (9)$$

$$E[q^2] = \frac{\Delta^2}{12}. \quad (10)$$

This treatment is valid for complex input signals whose amplitudes are large relative to the quantization step $\Delta$. However, it fails catastrophically for small or simple signals.

### B. Dither

Dither, which is an intentionally applied form noise, can decorrelate signal-dependent noise, has been widely applied to suppress the quantization effects on audio or video signal processing [6], [7]. There exist two archetypes of dithering systems: subtractively dithered system and nonsubtractively dithered system. Their schematics are shown in Fig. 6. In the subtractively dithered system, the total error is expressed by

$$\begin{aligned} e &= y - x \\ &= Q(x+\nu) - (x+\nu) \\ &= q(x+\nu), \end{aligned} \quad (11)$$

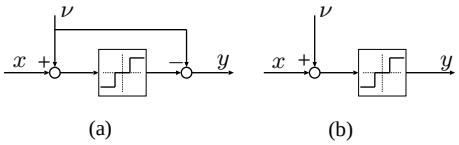


Fig. 6. Dithering systems. (a) Subtractively dithered system; (b) Nonsubtractively dithered system. $x$ is the system input, and $y$ is the system output.

where $\nu$ denotes the dither. Note that the dither $\nu$ can be chosen to control the properties of the error $e$. In particular, it can be shown that [6]:

*Schuchman's Condition:* In a subtractively dithered quantizing system, the total error $e$ is uniformly distributed and statistically independent of the input for arbitrary input distributions if and only if the characteristic function of the dither, $P_\nu$, satisfies the condition that

$$P_\nu(u)|_{u=k/\Delta} = 0, \quad \text{for } k = \pm 1,\ \pm 2,\ \pm 3, .... \tag{12}$$

The characteristic function of a random variable is the Fourier transform of its pdf $p$, which is defined by

$$P(u) \triangleq \int_{-\infty}^{\infty} p(\epsilon) e^{-j2\pi u\epsilon} d\epsilon. \tag{13}$$

Note that a dither with the uniform probability distribution

$$p_\nu(\epsilon) = \begin{cases} \frac{1}{\Delta}, & -\frac{\Delta}{2} < \epsilon \le \frac{\Delta}{2} \\ 0, & \text{otherwise,} \end{cases} \tag{14}$$

has the corresponding characteristic function

$$P_\nu(u) = \frac{\sin(\pi\Delta u)}{\pi\Delta u}, \tag{15}$$

which satisfies the desired condition (12). Applying this sort of dither can made the total error $e$ be independent of input $x$. In addition, the mean and the variance of the total error $e$ are as same as (9) and (10) [6].

Subtractively dithered systems are clearly ideal in the sense that they render the total error $e$ be independent of the input. The requirement of synchronous dither subtraction at the system output, however, cannot always be implementable in practical situations. It is for such reason, nonsubtractive dither technique introduced in the following is also of interest.

In the case of nonsubtractively dithered system, the total error can be given by

$$\begin{aligned} e &= y - x \\ &= Q(x+\nu) - x \\ &= q(x+\nu) + \nu. \end{aligned} \tag{16}$$

Obviously the total error is not simply the quantization error alone, but also involves the dither. Unlike subtractive dithering method, it is shown that nonsubtractive dithering method cannot make the total error be statistical independent of the system input, but the following result can be obtained [7]:

*Theorem:* In a nonsubtractively dithered quantizing system,

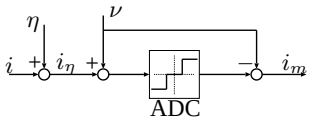


Fig. 7. Model of subtractive dithering method for current quantization.

$E[e^l|x]$ is functionally independent of the input $x$ for $l = 1, 2, ..., M$ if and only if

$$\frac{d^i P_\nu}{du^i}(u)\ \Big|_{u=k/\Delta} = 0 \quad \text{for } k = \pm 1, \pm 2, \pm 3, ..., \tag{17}$$

where $i = 0, 1, 2, ..., M-1$.

It is analyzed in [8] that triangular-pdf dither

$$p_\nu(\epsilon) = \begin{cases} \frac{1}{\Delta^2}(\epsilon + \Delta), & -\Delta < \epsilon \le 0 \\ \frac{1}{\Delta^2}(-\epsilon + \Delta), & 0 < \epsilon \le \Delta \\ 0, & \text{otherwise,} \end{cases} \tag{18}$$

whose characteristic function is

$$P_\nu = \left( \frac{\sin(\pi\Delta u)}{\pi\Delta u} \right)^2, \tag{19}$$

is unique choice to render the mean and the variance of the total error $e$ be independent of the input, while minimizing the spectrum of the total error $e$. In this case, the mean and variance are expressed by

$$E[e] = 0, \tag{20}$$

$$E[e^2] = \frac{\Delta^2}{4}. \tag{21}$$

## III. Dithering techniques and Kalman filter for current quantization

In this section, a current control system for a surface PM synchronous motor is considered. Dithering techniques are applied to whiten the quantization noise by taking into account the statistical properties of the metering noise. Then, Kalman filter is exploited to estimate the real current signal based on the whitened measurement error.

### *A. Subtractively dithered system*

In this case, the traditional subtractively dithered method is exploited to whiten current quantization error, and its application is shown in Fig. 7. The current error is expressed as

$$\begin{aligned} e_i &= i_m - i \\ &= Q(i_\eta + \nu) - (i_\eta + \nu) + \eta \\ &= q(i_\eta + \nu) + \eta. \end{aligned} \tag{22}$$

According to *Schuchman's Condition*, $q(i_\eta + \nu)$ is independent of $i_\eta$ if $\nu$ is uniform in $[-\frac{\Delta}{2}\ \frac{\Delta}{2}]$. Therefore, if the metering noise $\eta$ can be assumed to be white noise, the total current measurement error $e_i$ would be regarded as white noise. The mean and the variance of $e_i$ are expressed as

$$E[e_i] = 0, \tag{23}$$

$$E[e_i^2] = E[\eta^2] + \frac{\Delta^2}{12}. \tag{24}$$

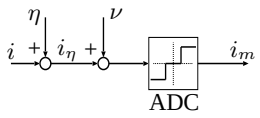


Fig. 8. Model of nonsubtractive dithering method for current quantization.

### B. Nonsubtractively dithered system

The application of nonsubtractively dithered system is shown in Fig. 8. Though the traditional nonsubtractively dithered method can be applied for whitening the quantization error, the variance of the total error is

$$E[e_i^2] \quad = \quad E[\eta^2] + \frac{\Delta^2}{4}, \tag{25}$$

which may be too large to be allowed. Therefore, the properties of the metering noise $\eta$ is considered. In other words, in order to minimize the spectrum of total error as well as whitening the quantization noise, the nonsubtractive dither is designed based on the pdf of $\eta$. Denote the sum of the dither $\nu$ and the metering noise $\eta$ by

$$w \triangleq \eta + \nu. \tag{26}$$

According to the *Theorem*, the optimal selection of $v$ is the one which can control $w$ to have the same pdf as the triangular-pdf noise (18). Assuming that $\eta$ is zero-mean and has the variance less than the triangular-pdf noise (18), a theoretical selection of $\nu$ is

$$p_\nu = \boldsymbol{\mathcal{F}}^{-1} \frac{\text{sinc}^2(\pi\Delta u)}{P_\eta(u)} du, \tag{27}$$

according to the convolution theorem and inverse Fourier Transform. $\text{sinc}^2(\pi\Delta u)$ and $P_\eta(u)$ are the characteristic function of triangular-pdf (18) and $\eta$, respectively. By this way, $w$ has the same pdf as the triangular-pdf noise (18), and the variance of the total error is

$$E[e_i^2] = \frac{\Delta^2}{4}. \tag{28}$$

This implies that the variance is not affected by $\eta$ and smaller than (25). However, $\nu$ with the pdf obtained from (27) is usually not easy for implementation. According to the practical situation, a common case that $\eta$ is Gaussian noise is discussed.

*1) The metering noise is Gaussian noise:* In this case, determining $\nu$ based on (27) is very hard not only because of the calculation, but also the realization for practical situation. Therefore, designing $\nu$ to make the pdf of $w$ be approximated with (18) is considered. For the simplicity on implementation, and according to the convolution theorem, the following result can be obtained:

*Proposition 1:* Suppose that the metering noise $\eta$ is Gaussian noise and has the Normal distribution:

$$p_\eta(\epsilon) = \frac{1}{\sqrt{2\pi\sigma^2}} e^{-\frac{1}{2}\frac{\epsilon^2}{\sigma^2}}, \quad 0 < \sigma^2 < \frac{\Delta^2}{6}, \tag{29}$$

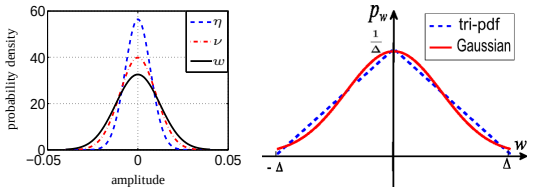


Fig. 9. (a): Example of $w = \eta + \nu$ from the viewpoint of probability density when $\eta$ and $\nu$ are Gaussian. (b): The comparison of triangular-pdf and Gaussian distribution with the same variance.

where $\sigma$ is its standard deviation, then $w$ is also Gaussian and has the same variance with (18) if the distribution of $\nu$ satisfies

$$p_\nu(\epsilon) = \frac{1}{\sqrt{2\pi(\frac{\Delta^2}{6} - \sigma^2)}} e^{-\frac{1}{2}\frac{\epsilon^2}{\frac{\Delta^2}{6} - \sigma^2}}. \tag{30}$$

$\frac{\Delta^2}{6}$ is the variance of triangular-pdf (18). If $\sigma^2 \geq \frac{\Delta^2}{6}$, it can be regarded as that $\eta$ is large enough to whiten the quantization noise and the dither $\nu$ is not necessary. Fig. 9(a) illustrates the sum of two variables from the view point of pdf.

It can be calculated that the approximation error between Normal distribution and the triangular distribution (18) between $[-\Delta \ \Delta]$ is about 10% when they have the same variance. Fig. 9(b) indicates the comparison of the probability density functions.

### C. Kalman filter

In this subsection, Kalman filter is designed to reduce the effects caused by the whitened noise. The model of SPMSM can be expressed as (4) by applying the decoupling control. One state-space realization of (4) is expressed as

$$\dot{\boldsymbol{x}} = \boldsymbol{A}\boldsymbol{x} + \boldsymbol{B}\boldsymbol{u}, \tag{31}$$

$$\boldsymbol{y} = \boldsymbol{C}\boldsymbol{x}, \tag{32}$$

where $\boldsymbol{y} = \boldsymbol{x} = [i_u \ i_v \ i_w]^T$, $\boldsymbol{u} = [v'_u \ v'_v \ v'_w]^T$ and

$$\boldsymbol{A} = \begin{bmatrix} -\frac{R}{L} & 0 & 0 \\ 0 & -\frac{R}{L} & 0 \\ 0 & 0 & -\frac{R}{L} \end{bmatrix}, \boldsymbol{B} = \frac{2}{3L} \begin{bmatrix} 1 & -\frac{1}{2} & -\frac{1}{2} \\ -\frac{1}{2} & 1 & -\frac{1}{2} \\ -\frac{1}{2} & -\frac{1}{2} & 1 \end{bmatrix},$$

$$\boldsymbol{C} = \begin{bmatrix} 1 & 0 & 0 \\ 0 & 1 & 0 \\ 0 & 0 & 1 \end{bmatrix}.$$

Based on this model, the current signals estimation based on Kalman filter is formed as

$$\dot{\hat{\boldsymbol{x}}} = \boldsymbol{A}\hat{\boldsymbol{x}} + \boldsymbol{B}\boldsymbol{u} + \boldsymbol{L}_k(\boldsymbol{y} - \boldsymbol{C}\hat{\boldsymbol{x}}), \tag{33}$$

where $\boldsymbol{L}_k$ is usually referred to Kalman gain, and calculated by $\boldsymbol{L}_k = \boldsymbol{P}\boldsymbol{C}^T\boldsymbol{R}_c^{-1}$. $\boldsymbol{R}_c$ is the covariance of measurement noise and $\boldsymbol{P}$ is the solution of following Riccati equation

$$\boldsymbol{A}\boldsymbol{P} + \boldsymbol{P}\boldsymbol{A}^T - \boldsymbol{P}\boldsymbol{C}^T\boldsymbol{R}_c^{-1}\boldsymbol{C}\boldsymbol{P} + \boldsymbol{Q}_c = \boldsymbol{0}, \tag{34}$$

where $\boldsymbol{Q}_c$ is the covariance of input disturbance.

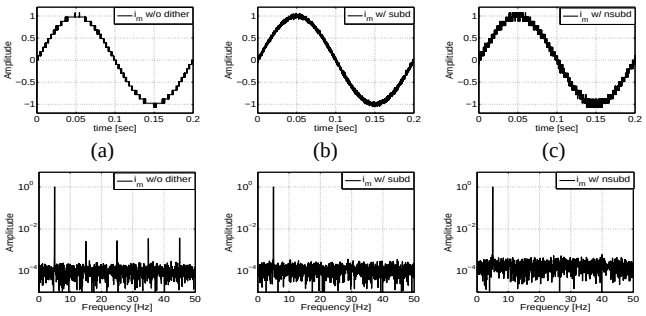


Fig. 10. Comparison of simulation results. (a), (d) shows the measured signal and its feature without applying dither. (b), (e) shows the result when subtractive dither is applied. (c), (f) shows the result when nonsubtractive dither is applied.

## IV. Simulations

In this section, the simulations are performed to verify the effectiveness of the dithering techniques. An ADC with a resolution of 10-bit and a measurement range of $\pm 50$A is considered. The quantization step is $\Delta = 50/2^9$. The input current signal is set as $i = \sin 10\pi t$. The metering noise $\eta$ is set as that it has a Normal probability density function $N(0, \frac{\Delta^2}{48})$. Without dither, with the subtractive dither designed by (14), and with the nonsubtractive dither designed by (30) are examined. The simulation results are shown in Fig. 10. Fig. 10(a–c) show the individual outputs and Fig. 10(d–f) show the FFT analysis results of outputs, respectively. It is observed that the fundamental harmonic is only remained and the harmonics caused by quantization are suppressed when dithering techniques are applied. Therefore, the effectiveness of the subtractive dithering method and the nonsubtractive dithering method is verified.

## V. Experiments

In this section, the effectiveness of the dither techniques and Kalman filter is verified via experiments. A linear stage is used, as shown in Fig. 11(a). The parameters are shown in Table. I. The stage is driven by linear motors located at the both sides of the carrier. DSP(TMS320C6713, 225MHz) is used as the processor. Current signals are measured by FA-050PV whose measurement range is $\pm 50$A. The current signals are converted into digital signals by high-precise A/D converters whose resolution is 14-bit. The resolution is dropped to 10-bit by software for experiments and the quantization step is $\Delta = 0.0977$ A. Dither is generated by DSP and then converted to analog signals via the D/A converters whose resolution is 16-bit. The implementation of dithering techniques is shown in Fig. 11(b). A time delay is introduced to synchronize the addition and the subtraction in the case that subtractively dithered method is used. VSPTC with SRC method [10] is used to design outer loop controllers to generate current reference. Vector control method with pole-zero cancellation current controller is applied. The block diagram of control system is shown in Fig. 12. Decoupling control is exploited

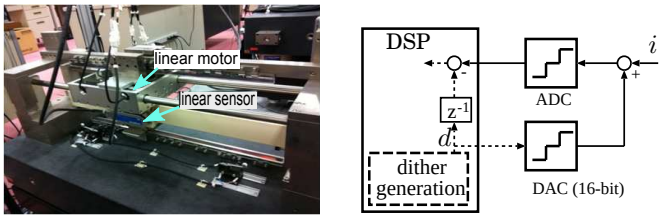


Fig. 11. Experimental setup (a) and implementation of dithering techniques (b).

TABLE I
Parameters of Stage

| | | |
|---|---|---|
| Inductance $L$ | $15.5 \times 10^{-3}$ | H |
| Resistance $R$ | 20.5 | $\Omega$ |
| Mass $M$ | 14.5 | kg |
| Viscosity $B$ | 24 | N/(m/s) |
| Thrust coefficient $K_t$ | 26.5 | N/A |
| Bach-EMF constant $K_e$ | 16 | V/(m/s) |

for linearizing the plant. For comparison, the cases that without dither, with subtractive dither and with nonsubtractive dither are examined, respectively. Kalman filter is applied if the switch is turned to 'a'.

Firstly, the probability distribution of the metering noise is analyzed. A sample of metering noise in time domain is shown in Fig. 13(a). Its histogram plot is shown in Fig. 13(b). It is observed that the metering noise can be approximated with Gaussian noise, and the corresponding variance is Var $= 1.1218 \times 10^{-4}$. Based on this data, the nonsubtractive dither and subtractive dither are designed according to (30) and (14). Kalman gain $L_k$ is designed based on the error variances (24) and (28), and the convergence bandwidth of the estimation is 400Hz.

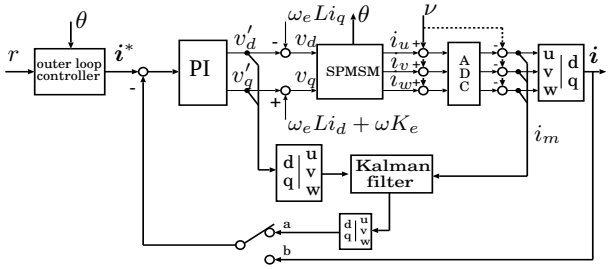


Fig. 12. Block diagram of control system.

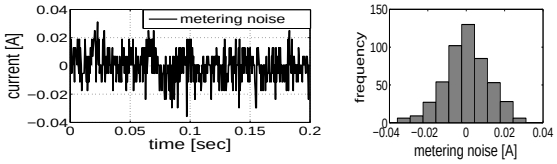


Fig. 13. Example of the metering noise (a) and its histogram analysis (b).

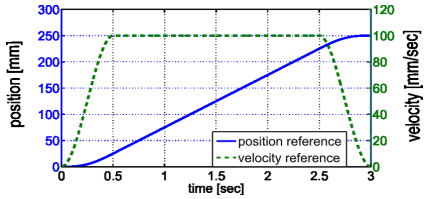


Fig. 14. Position and velocity reference.

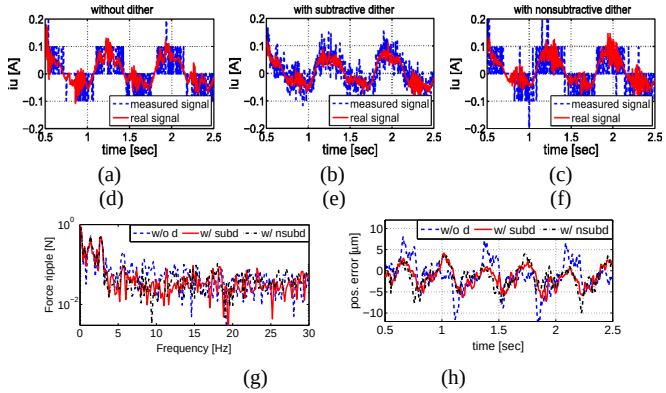


Fig. 15. Experimental results without Kalman filter. (a), (b) and (c) show the comparisons of measured U-phase current signal and real U-phase current signal, respectively. (d), (e) and (f) show the resulting power spectral density of measured current errors. (g) shows the comparison of the force ripple. (h) shows the comparison of position tracking error.

In the setup, the trajectory reference is set as Fig. 14. For the simplicity of comparison, the step that the stage moves at a constant speed (0.5s∼2.5s) is examined. Fig. 15 shows the results that Kalman filter is not applied. In the figure,(a), (b) and (c) show the comparisons of measured U-phase current signal and real U-phase current signal, respectively. (d), (e) and (f) show the resulting power spectral density of measured current errors. (g) shows the comparison of the force ripple. It can be observed that the components at high frequencies are reduced by dithering techniques. The position tracking error can also be reduced by applying dithering techniques, which is shown in (h). Fig. 16 shows the results when Kalman filter is applied. In this figure, (a), (b) and (c) show the real U-phase current signals and (d) shows the comparison of the position tracking error. Compared with Fig. 15, it is obtained that the current signals are much smoother and the high-harmonic current components are reduced. The RMS of the position tracking errors are shown in Table II. It is demonstrated that combining the dithering techniques and Kalman filter can improve the control performance.

TABLE II
THE RMS OF TRACKING ERROR WITH & WITHOUT DITHER

| tracking error ($\mu m$) | w/o d | w/ subd | w/ nsubd |
|---|---|---|---|
| w/o Kalman filter | 3.8118 | 2.8307 | 3.0078 |
| w/ Kalman filter | 3.0167 | 2.7741 | 2.7851 |

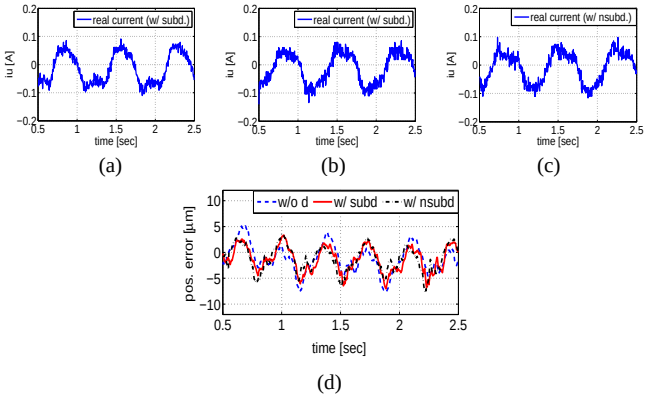


Fig. 16. Experimental results of Kalman filter. (a), (b) and (c) show the real U-phase current signals. (d) shows the comparison of the position tracking error.

## VI. CONCLUSION

In this paper, the combining of dithering techniques and Kalman filter for suppressing current quantization noise are presented. The simulation results and experimental results show the effectiveness of the proposed methods. It is concluded that the quantization noise can be whitened by deliberately designed dither, and the whitened noise can further be reduced by Kalman filter.

## ACKNOWLEDGMENT

This work was partially supported by Global COE Program ”Secure-Life Electronic”, MEXT, Japan.

## REFERENCES

[1] J. Holtz, and J. Quan, Sensorless Vector Control of Induction Motors at Very Low Speed Using a Nonlinear Inverter Model and Parameter Identification, *IEEE Trans. Indust. appl.* , Vol. 38, No. 4, pp. 1087–1095, Jul./Aug. 2002.

[2] K. Nakamura, H. Fujimoto, and M. Fujisuna, Torque Ripple Suppression Control for PM Motor Considering the Bandwidth of Torque Meter (in Japanese), *IEEJ Trans. IA* , Vol. 130, No. 11 pp. 1241–1247, 2010.

[3] J.H. Jang, S.K. Sul, and Y.C. Son, Current Measurement Issues in Sensorless Control Algorithm using High Frequency Signal Injection Method, *Proc. IEEE Ind. App. Soc. Annual Meeting* , Vol.2 pp. 1134–1141, Oct. Salt Lake City, 2003.

[4] A. S. Hodel, and J. Y. Hung, A State Estimator with Reduced Sensitivity to Sensor Quantization, *IECON03*, pp. 586–590, 2003.

[5] A. Molin, and S. Hirche, On LQG Joint Optimal Scheduling and Control under Communication Constraints, *Joint 48th IEEE Conference on Decision and Control and 28th Chinese Control Conference* , pp. 5832–5838, Shanghai, Dec. 2009.

[6] L. Schuchman, Dither Signals and Their Effect on Quantization Noise, *IEEE Trans. Commun. Technol.* , pp. 162–165, Decr. 1964.

[7] S.P. Lipshitz, R.A. Wannamaker, and J. Vanderkooy, Quantization and Dither: A Theoretical Survey, *J. Audio Eng. Soc.* , Vol. 40, No.5, pp. 355–375, May 1992.

[8] R.A. Wannamaker, S.P. Lipshitz, J. Vanderkooy,and J.N. Wright, A Theory of Nonsubtractive Dither, *IEEE Trans. Signal Processing* , Vol. 48, No.2, pp. 499–516, Feb. 2000.

[9] B. Widrow, I. Kollár, and M. Liu, Statistical Theory of Quantization, *IEEE Trans. Instrum. Meas.*, Vol. 45, No. 2, pp. 353–361, Apr. 1996.

[10] K. Sakata, H. Fujimoto, High Bandwidth Design of Feedback Control System Using Multiple Sensors for High-Precision Stage, *Proc. The 39th SICE Symposium on Control Theory* , pp. 285-290, 2010 (in Japanese).